Results on the Total Hadronic Cross Section and Four-Prong Production in Photon-Photon Interactions.

PEP-4 TPC/PEP-9 TWO-GAMMA COLLABORATION[1,2]

F.C.ERNÉ.

National Institute for Nuclear and High Energy Physics, Amsterdam, The Netherlands.

I. Introduction

The assumption of vector dominance for both photons in gamma-gamma collisions leads us to expect a certain analogy with hadron-hadron scattering. Elastic scattering and charge exchange would lead to the production of pairs of neutral and charged vector mesons, and the simplest quantity one can define, the total cross section, would be predictable from factorization with photon-nucleon and nucleon-nucleon scattering total cross sections. Below we will discuss measurements that test this assumption.

Collisions at PEP and at similar e^+e^- colliders offer a variety of ways to define the $\gamma\gamma$-collision c.m. energy. In the total cross section measurement[1] we determine it by accurately tagging the electrons and positrons scattered in the forward direction, while the reaction products are only partially observed. In this way the efficiency of observing the occurrence of an event is high (40 - 100%) and relatively free from biases. In the case of vector-meson production[1,2] we measure the c.m. energy from the reaction products, with constraints on the observed events to ensure their exclusive character. Here the detection efficiency is low (typically 10%).

We will discuss measurements of:

i) the total hadronic cross section in doubly tagged data,

ii) a) ϕ and $K^{*0}(890)$ production in $\gamma\gamma \rightarrow K^+K^-\pi^+\pi^-$ in untagged data, and
b) the dependence of the cross section for $\gamma\gamma \rightarrow \pi^+\pi^-\pi^+\pi^-$ on the invariant mass of one of the colliding photons in singly tagged data.

The data, collected at PEP at an e^+e^- c.m. energy of 29 GeV, correspond to an integrated luminosity of 50 pb^{-1}.

II. Apparatus

The PEP-4/PEP-9 detector system at the e^+e^- colliding beam facility PEP at SLAC has been described earlier.[3] The angular coverage of the detector is optimized for two-photon physics; tracks can be recognized at angles between 22 and 180 mrad and between 280 mrad and $\pi/2$ with respect to either beam. A side view of the experiment is shown in Fig. 1. We summarize here the features of the detector which are important for the present investigation.

Detection of the tagging electron or positron at small angles is achieved in two arrays of NaI counters, each containing 60 crystals with a resolution of 1.5% at 14.5 GeV, covering the angular range between 22 and 90 mrad, and with lead/scintillator shower counters with coordinate readout in three projections between 100 and 180 mrad. Charged particles in the forward spectrometers are tracked by 15 drift chambers through a septum magnet ($\int Bdl = 0.24$ Tm). At angles above 180 mrad the lead/proportional chamber pole-tip calorimeters (PTC) of the central system detect tagging electrons at angles between 280 and 620 mrad. The remaining solid angle is covered by hexagonal Geiger-mode calorimeters (HEX) outside the magnet coil.

The heart of the central detector is the Time Projection Chamber (TPC) operating in a 0.4 T magnetic field in which charged particles are identified by ionization loss (dE/dx) over almost the entire solid angle. The momentum

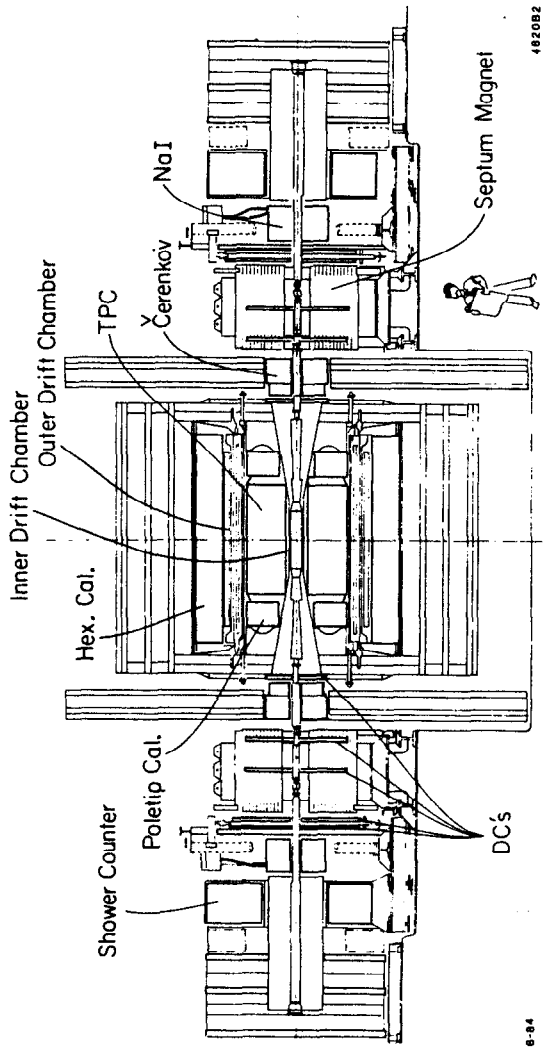

***Fig.1* : Side view of the PEP-4 TPC/PEP-9 apparatus.**

resolution at large angles is $(\delta p/p)^2 = (0.06)^2 + (0.035p)^2$ (p in GeV). Tracks from charged particles are also recorded in a four-layer inner drift chamber (IDC) placed around the beam pipe within the TPC pressure vessel and in a three-layer outer drift chamber (ODC) placed around the magnet coil.

III. Total Cross Section

A measurement of the total hadronic cross section in photon-photon collisions is reported for center-of-mass energy, W, between 2 and 20 GeV. This cross section is studied via the process $e^+e^- \rightarrow e^+e^-\gamma^*\gamma^* \rightarrow e^+e^-+$ hadrons. The present measurement uses events in which both the scattered e^+ and e^-, referred to as tags, are detected. The four momentum and polarization mixture of each virtual photon are thus known. The photon four momentum squared, $Q^2_{1,2}$, is taken as a positive quantity. For this measurement it is between 0.1 and 1.6 GeV^2. The photon-photon collision and W axis are determined on an event-by-event basis directly from the tags. A previously reported measurement[4] using single-tagged events inferred the W spectrum of the observed events from the W spectrum of the detected hadrons. Double tagging eliminates the need for this procedure but considerably reduces event yield. Finally, tagging both virtual photons permits the measurement of interference between photon helicity states.

The cross section for $e^+e^- \rightarrow e^+e^-+$hadrons is given by[5]

$$E_1'E_2'\frac{d^6\sigma}{d^3p_1'd^3p_2'} = L_{TT}(\sigma_{eff} + \frac{1}{2}\epsilon_1\epsilon_2\tau_{TT}cos2\tilde{\phi}+ + 2\sqrt{\epsilon_1(1+\epsilon_1)\epsilon_2(1+\epsilon_2)}\tau_{TS}cos\tilde{\phi}) \quad \text{(III.1)}$$

where

$$\sigma_{eff} \equiv \sigma_{TT} + \epsilon_2\sigma_{TS} + \epsilon_1\sigma_{ST} + \epsilon_1\epsilon_2\sigma_{SS} \quad . \tag{III.2}$$

Here $(E_i', \vec{p}_i')$ is the four momentum of tag i, and $\tilde{\phi}$ is the acoplanarity (angle between e^+ and e^- scattering planes) in the $\gamma^*\gamma^*$ center of mass. The subscripts T and S refer to transverse and scalar photons respectively. The virtual photon flux factor, L_{TT}, and ϵ_1 and ϵ_2 (photon polarization parameters) are given exactly by QED. The quantities of interest are the four $\gamma^*\gamma^*$ cross sections (σ_{ab}) and two interference intensities (τ_{ab}). They are functions of W, Q_1^2 and Q_2^2 only. In the present investigation, ϵ_1 and ϵ_2 are generally near 1, and the σ_{ab} have been grouped into the effective cross section given in Eq.(III.2). QED requires that for $Q_i^2 \to 0$ $(i = 1,2)$:

$$\sigma_{TS} \propto Q_2^2, \quad \sigma_{ST} \propto Q_1^2, \quad \sigma_{SS} \propto Q_1^2Q_2^2, \quad \tau_{TS} \propto \sqrt{Q_1^2Q_2^2} \quad . \tag{III.3}$$

Further $\tau_{TT} = \sigma_{\parallel} - \sigma_{\perp}$, where $\sigma_{\parallel}$ and $\sigma_{\perp}$ are cross sections for the collision of transverse photons with relatively parallel and perpendicular polarizations, respectively.

The trigger used in this investigation required an energy deposition greater than 0.8 GeV in each of the two NaI calorimeters.[6] Requiring the depositions to be acolinear with the interaction point reduced triggers due to elastic e^+e^- (Bhabha) scattering by a factor of 25.

In the analysis, events were selected that have a tag with an energy greater than 3 GeV in each of the NaI calorimeters. In addition, the laboratory acoplanarity angle of the tags was required to be greater than 0.55 radians to reduce backgrounds from the reaction $e^+e^- \to e^+e^-\gamma$. Hadronic events were selected by requiring a minimum total detected multiplicity of 3 particles (excluding the tags), with at least 2 being charged. The charged multiplicity included tracks only if they originated at the event vertex and had a momentum greater than 200 MeV/c in the forward spectrometers or 50 MeV/c in the TPC. The neutral multiplicity included calorimeter depositions greater than 300 MeV, isolated from any charged track. Additionally at least one charged track had to be identified as a hadron (or hadron/muon ambiguity), primarily using dE/dx in the TPC and E/p measurements. A total of 790 events was thus selected as hadronic. Based on visual scanning, corrections ranging from 10 for $W < 4$ to 0 for $W > 11$ GeV were applied for residual electromagnetic events. Without the requirement of an identified hadron the background from electromagnetic events would have been as large as 40% at low W. A correction of 14% for $W > 15$ decreasing to 0 for $W < 10$ GeV was applied for single-tagged events appearing as double-tagged events. This correction was determined by observing events with like-sign tags where the tag of incorrect sign was caused by a hadron or pair produced lepton. The contribution of $\gamma\gamma \to \tau\bar{\tau}$ with subsequent decays $\tau \to$ hadrons, calculated to be less than 6% for $3 < W < 8$ GeV and negligible at all other W, has been subtracted from the data.

To obtain the total cross section and related distributions, a Monte Carlo simulation was performed using Eq. (III.1), with constant σ_{eff}, τ_{TT} and τ_{TS} terms, and the hadronic state model described below. Event selection and the acceptances and resolutions of the various detectors were simulated. Radiation by the incident electron and positron was taken into account following Tsai.[7]

The resulting Monte Carlo W resolution agrees well with the resolution observed in $ee \to ee\mu\mu$ data events ($\sigma_W \simeq$ 0.8 GeV at $W = 2$ GeV, $\simeq 0.5$ GeV for $W \geq$ 10 GeV).

The detection efficiency for the produced hadronic state is sensitive to the charged multiplicity, but is largely insensitive to other characteristics of the final state. The simulation's charged multiplicity distribution as a function of W was adjusted to agree with the data. The number of $\pi^+\pi^-$ pairs and, independently, π^0's were generated according to a Poisson distribution with an average of $0.5 + 0.26W$. For a given simulated W, multiplicities of fewer than 3 pions were not generated. Thus all hadrons are assumed to be pions, charge is conserved and the average numbers of π^+, π^- and π^0 are equal. Each pion was generated with a limited p_t^2 with respect to the $\gamma^*\gamma^*$ collision axis, as invariant phase space times $\exp(-{p_t}^2/0.4^2)$. This particular p_t^2 distribution was chosen to obtain agreement with the data at low p_t^2. Excesses in the data at $p_t^2 \geq 0.5$ GeV$^2/c^2$ are observed but have a negligible effect upon the extracted value of the total cross section. The detection efficiency as calculated from the simulation is shown in Fig. 2 as a function of W.

The experimental separation of σ_{eff}, τ_{TT} and τ_{TS} in (III.1) is based on the observed $\tilde{\phi}$ dependences. The ratios of τ_{TT} and τ_{TS} to σ_{eff} are determined, averaged over W and Q^2, by fitting the Monte Carlo $\tilde{\phi}$ distributions for the three terms to the data. Values of $\tau_{TT}/\sigma_{eff} = -0.49 \pm 0.24$ and $\tau_{TS}/\sigma_{eff} = -0.02 \pm 0.04$ are found. No W dependence is observed.

The value of τ_{TT}/σ_{eff} given above indicates that $\sigma_\perp$ is larger than $\sigma_\parallel$. The small value of τ_{TS} at the low average Q^2 of the data is not surprising considering

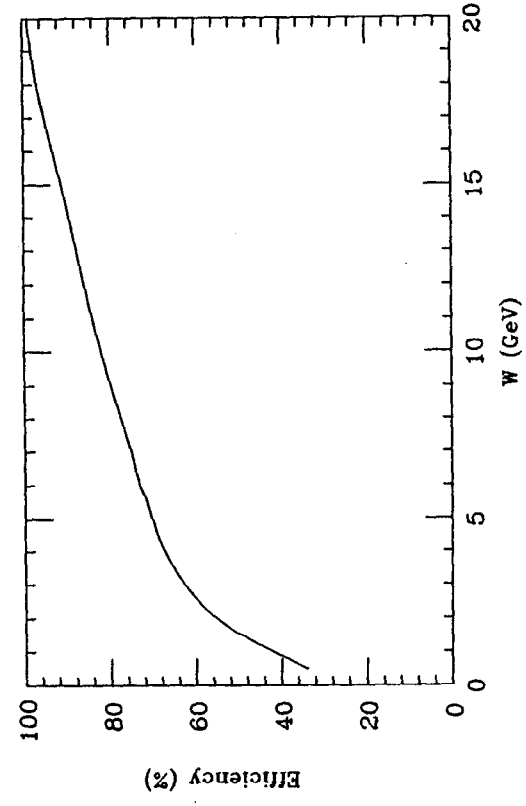

Fig.2: Efficiency for the detection of the hadronic state including effects of hadron selection.

Eq. (III.3). After integration over $\tilde{\phi}$, τ_{TT} and τ_{TS} terms contribute no more than 5% to the total cross section. The remaining term in Eq.(III.1), σ_{eff}, is hereafter referred to as $\sigma_{\gamma\gamma\to\text{had}}$.

Comparison of the data to the Monte Carlo simulation (with $\tau_{TT} = \tau_{TS} = 0$) allows extraction of the Q^2 and W dependences of $\sigma_{\gamma\gamma\to\text{had}}$. Figure 3 shows $\sigma_{\gamma\gamma\to\text{had}}$ as a function of Q^2_{max} (the larger of each event's two $|Q_i^2|$) for three regions of W. The data have been averaged over Q^2_{min} (the smaller of the two $|Q_i^2|$). The curves of Fig. 3 assume that each term of Eq. (III.2) factorizes as

$$\sigma_{ab}(Q_1^2, Q_2^2, W) = f_a(Q_1^2) f_b(Q_2^2) \sigma_0(W), \qquad \text{(III.4)}$$

where a and b are T or S. One set of curves takes f_T and f_S from a Generalized Vector Meson Dominance (GVD) model[8] with parameters chosen to describe inelastic ep scattering, the other from a simple ρ-dominance model.[9] The latter model does not agree with the data (χ^2/df= 36/12) while the GVD model is in good agreement (χ^2/df= 17/12). The Q^2_{min} dependence (not shown) leads to the same conclusion.

In Fig. 4 the GVD model is used to interpolate $\sigma_{\gamma\gamma\to\text{had}}$ to $Q_1^2 = Q_2^2 =$ 0.3 GeV^2 and $\epsilon_1 = \epsilon_2 = 1$ (left scale), and to extrapolate it to $Q_1^2 = Q_2^2 = 0$ (right scale). Results for $W < 2$ GeV are not shown due to increased W smearing, non-statistical multiplicity distributions and the presence of resonances. The shaded band for this experiment in Fig. 4 is a one standard deviation envelope for $\sigma_{\gamma\gamma\to\text{had}}(W)$ assuming a parametrization of the form $a + b/W$. At $Q_1^2 = Q_2^2 = 0$ the fitted values are $a = 360 \pm 60\ nb$ and $b = 10 \pm 290\ nb$ GeV with a correlation coefficient of −0.92. The above fit was performed utilizing the Monte

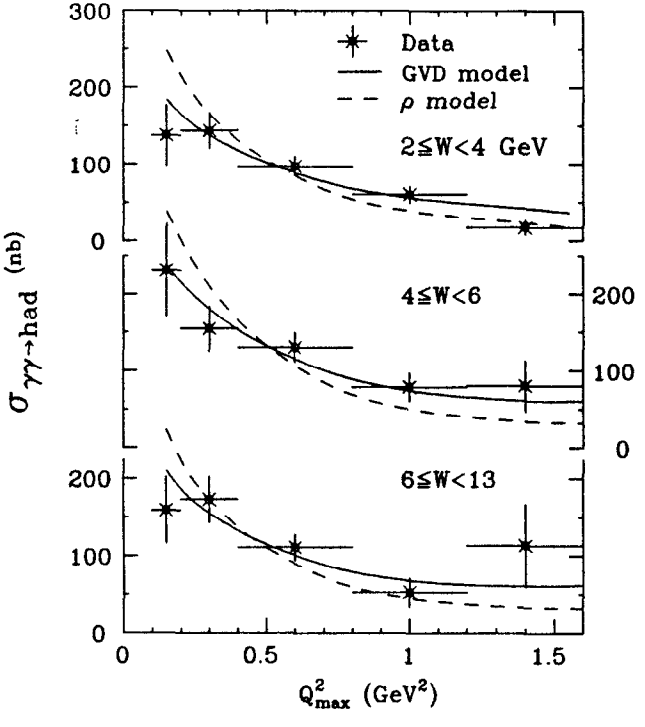

Fig.3 : The $\sigma_{\gamma\gamma\to\text{had}}$ vs Q^2_{max}, averaged over Q^2_{min}, in three W bins (counting errors only).

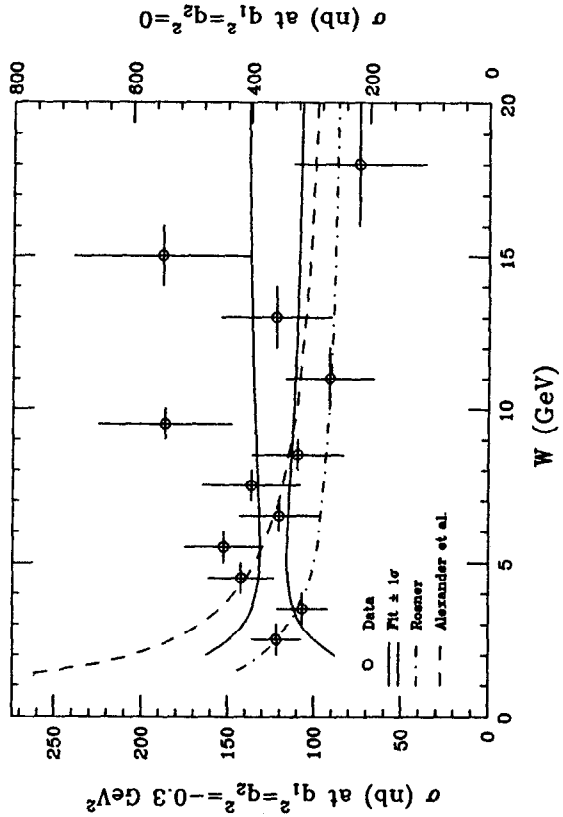

Fig.4 : The $\sigma_{\gamma\gamma\to\text{had}}$ vs W, interpolated to $Q^2_1{=}Q^2_2{=}$ 0.3 GeV^2 and $\epsilon_1 = \epsilon_2 = 1$ (left scale) and extrapolated to $Q^2_1{=}Q^2_2{=}0$ (right scale). The band for this experiment represents the $\pm 1\sigma$ boundaries of the fit described in the text. Data point errors are counting errors only.

Carlo simulation to account for W resolution effects. The data points of Fig. 4 are those extracted when the W dependence of the input cross section to the Monte Carlo is given by the fit.

Systematic uncertainties are 20% for W between 5 and 11 GeV, and 25% elsewhere. Effects considered were: (i) overall normalization; (ii) tag definition; and (iii) multiplicity modeling, particle counting and detector simulation.

Figure 4 shows the predictions for $\sigma_{\gamma\gamma\to\text{had}}$ at $Q^2_1 = Q^2_2 = 0$ from Refs. 10,11 to be in agreement with the data given the above systematic errors. It should be emphasized that the cross section reported here excludes final states of 2 hadrons. These could be significant below 3 GeV. If such states were included, assuming the Poisson distribution presented earlier, $\sigma_{\gamma\gamma\to\text{had}}$ would increase by 24% at W=2 GeV. We prefer to make no assumption about the 2 hadron states.

In conclusion, continuum hadron production in photon-photon scattering is observed at the level of 100-150 nb (at $Q^2{}_1{=}Q^2{}_2{=}$ 0.3 GeV^2) with only a small W dependence for $2 \leq$ W ≤ 20 GeV. Photon-photon scattering thus shows the characteristics of hadron-hadron collisions in its W dependence. Its Q^2 dependence is well described by a GVD model that also describes inelastic ep scattering.

IV. Vector Meson Production

An unexpectedly high cross section for the process $\gamma\gamma \rightarrow \pi^+\pi^-\pi^+\pi^-$ has been observed in several experiments.[12-15] The cross section is rising steeply at threshold and then falling off more slowly. The pair spectra show evidence of abundant $\rho^0\rho^0$ and $\rho^0\pi^+\pi^-$ as well as $\pi^+\pi^-\pi^+\pi^-$ phase space production with predominantly isotropic decay. A spin-parity analysis of the $\rho^0\rho^0$ component by the TASSO collaboration[13] indicated isotropic production and decay through a $J^{PC} = 0^{++}$ or 2^{++} state. The $J^{PC} = 0^{-+}$ and 2^{-+} disagree with measured angular distributions. In a related process, $\gamma\gamma \rightarrow \pi^+\pi^-\pi^0\pi^0$, the JADE collaboration[16] observed no such enhancement and established upper limits for the process $\gamma\gamma \rightarrow \rho^+\rho^-$.

The $\rho^0\rho^0$ and $\rho^+\rho^-$ measurements limit resonance models of the $\rho^0\rho^0$ enhancement to ones that allow interference between I=0 and I=2 amplitudes, as is seen by an isospin decomposition of the production amplitudes under the vector dominance hypothesis:

$$A(\rho^0\rho^0 \rightarrow \rho^0\rho^0) = \frac{2}{3}A(2) + \frac{1}{3}A(0)$$
$$A(\rho^0\rho^0 \rightarrow \rho^+\rho^-) = \frac{\sqrt{2}}{3}A(2) - \frac{\sqrt{2}}{3}A(0)$$

where A(0) and A(2) are the production amplitudes of the states in I=0 and I=2 respectively. For pure I=0 one expects

$$\sigma(\rho^+\rho^-) = 2\sigma(\rho^0\rho^0)$$

and for I = 2

$$\sigma(\rho^+\rho^-) = \frac{1}{2}\,\sigma(\rho^0\rho^0) \quad .$$

Neither case is observed experimentally.

Models compatible with the $\gamma\gamma \rightarrow \pi^+\pi^-\pi^+\pi^-$ data are of two types:

i) excitation of four-quark states. The existence of such states was postulated by Jaffe[17] and their excitation by $\gamma\gamma$ collisions was predicted by Li and Liu[18] and Achasov et al.[19] Jaffe classified the states in the MIT-bag model. In most cases the states are predicted to be very wide because of super allowed decays ; they "fall apart" into pseudoscalar or vector mesons. Close to threshold the width may be so small that the states become observable. In particular three $J^{PC} = 2^{++}$ states are predicted to be degenerate in mass at W $\approx$ 1.65 GeV, two with I = 0 and one with I = 2. Interference would give rise to the observed $\rho^0\rho^0$ and $\rho^+\rho^-$ cross sections.

ii) Pomeron + Reggeon exchange.[20] One could have

$$\eta, f, P \text{ exchange in } \gamma\gamma \rightarrow \rho^0\rho^0,$$
$$\pi^{+-}, {A_1}^{+-}, {A_2}^{+-} \text{ exchange in } \gamma\gamma \rightarrow {A_1}^{+-}\pi^{-+} \rightarrow \rho^0\pi^+\pi^-, \text{and}$$
$$\rho^{+-}, B^{+-} \text{ exchange in } \gamma\gamma \rightarrow \rho^+\rho^-.$$

Alternatively, factorization from photoproduction[21] predicts a sizable $\rho^0\rho^0$ cross section, but also a substantial cross section for $\gamma\gamma \rightarrow \omega\omega$.

For testing these models it is essential to investigate other vector meson pair production, such as $\phi\rho$, $\rho\omega$, $\omega\omega$ and $K^{*0}\overline{K}^{*0}$. Efforts to observe $\rho\omega$ and $\omega\omega$ have so far been unsuccessful.[22]

In this section the particle identification properties of the TPC detector are utilized to investigate $K^+K^-\pi^+\pi^-$ production in tagged and untagged events; furthermore we report on the Q^2 dependence of $\pi^+\pi^-\pi^+\pi^-$ production.

IV.1 DATA SELECTION

The event sample was obtained with two types of trigger:

— A coincidence of a tag in one of the forward calorimeters (E$\geq$ 2 GeV in the NaI or $\geq$ 8 GeV in a shower counter) and hits in at least two layers of the IDC. This rather loose trigger could not be used at tagging angles below 50 mrad, but imposed no constraint on the final state topology. Tagging angles between 30 and 50 mrad, as well as shower counter tags for which E$\geq$ 4 GeV, were covered by a trigger that also required hits in two layers of the ODC.

— A charged trigger in the TPC, required two tracks, each in a different 60 degree sector and at a polar angle greater than 30 degrees, and which projected back to the vertex to within 20 cm along the beam line. This trigger had no tag requirement.

In the off-line selection a tag was defined as a charged particle that deposited a minimum energy in an electromagnetic calorimeter. No magnetic momentum measurement was required for the tag, thus avoiding inefficiencies in the forward drift chambers and at small angles in the TPC. Tracks were required to come from the beam-beam intersection within 6 cm in radius and 10 cm along the beams.

For the untagged sample, two of the four tracks were required to have $p_\perp > 0.2$ GeV/c and all of the tracks satisfied $p_\perp > 0.120$ GeV/c and $|\cos\theta| < 0.87$. For the tagged sample, at least three of these tracks were to be recorded in the TPC. A forward track was required to be at angles between 22 and 180 mrad, and a central track at angles larger than 350 mrad with respect to one of the beams.

The dE/dx particle identification algorithm makes use of the truncated mean dE/dx, i.e., the lowest 65% of the samplings are retained. A χ^2 fit is made of this truncated mean and the measured momentum of the track to a theoretical dE/dx versus momentum curve for the various particle species. The fit value for species i is then χ^2_i. Only tracks for which there were at least 30 of a maximum of 180 dE/dx samples were used in the analysis.

The criteria used to obtain the $K^+K^-\pi^+\pi^-$ final state are the following: both kaons must be identified in the TPC, at least one kaon being unambiguously identified, i.e., $\chi^2_K + 4 < \chi^2_e$, χ^2_π, χ^2_p, and another particle being compatible with the kaon hypothesis, i.e., $\chi^2_K < 8$. In addition, one pion must be unambiguously identified, $\chi^2_\pi + 4 < \chi^2_e$, χ^2_K, χ^2_p, and the other particle must be compatible with the pion hypothesis, $\chi^2_\pi < 8$, if it is in the TPC. However, if the other identification requirements are satisfied, a particle in the forward arms of the detector, where there is no dE/dx information, is assumed to be a pion. Finally, a confidence level calculated for the $K^+K^-\pi^+\pi^-$ hypothesis for the event as a whole must be greater than 2%. Figure 5 shows the distribution of dE/dx versus momentum for the events identified as $K^+K^-\pi^+\pi^-$using this procedure.

The charges of pion and kaon pairs must sum separately to zero; and a minimum opening angle of 100 mrad is required between pairs to reject conversion electrons. To ensure the exclusivity of the event, a cut on $\Sigma p_\perp$ is made for both the untagged and tagged samples. A relatively large $\Sigma p_\perp$ is expected to occur from large angle tags, varying according to the tagging device resolution. We therefore required $\Sigma p_\perp < 0.3$ GeV/c perpendicular to the beam and tag

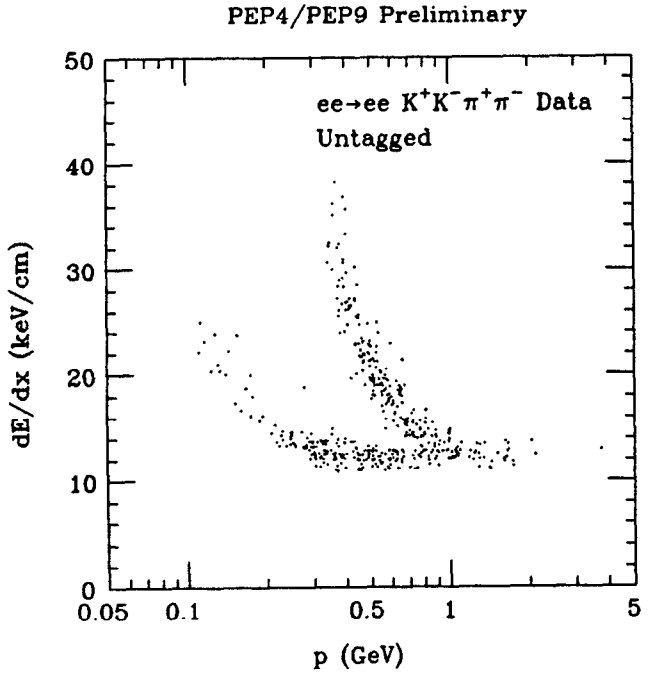

Fig.5 : The energy loss (dE/dx) versus momentum (p plot) for identified $K^+K^-\pi^+\pi^-$ events.

directions; the cut on $\Sigma p_\perp$ in the plane of the tag was variable, according to the resolution of the tagging device. For the untagged sample, we simply required $\Sigma p_\perp < 0.3$ GeV/c.

IV.2 Results

A cross section for the untagged sample has been calculated and is shown in Fig. 6. The calculation of the detector acceptance has been done using the equivalent photon approximation (EPA). Phase space production is assumed in generating the $K^+K^-\pi^+\pi^-$ system.

In a vector dominance model, one would expect $\phi\rho$ production, and this is also one of the vector-vector states expected from four-quark models. Figure 7 shows the mass spectra of the kaon pairs for the untagged and tagged samples. In both a clean ϕ peak can be observed. In Fig. 8, the mass spectra of the pion pairs from events without and with ϕ's are plotted. In neither case is there evidence for a ρ signal.

There is however a large $\phi\pi^+\pi^-$ signal. The acceptance calculation for this process at $Q^2 \approx 0$ depends sensitively on the details of the $p_\perp$ smearing, so the systematic errors are larger than in the $Q^2 \neq 0$ case and no cross section is given. From the tagged data one obtains, using the established branching fraction of ϕ to K^+K^-,

$$\sigma(\gamma\gamma \to \phi\pi\pi) = 6.6 \pm 4.1 \text{ nb}$$

for 0.15 $<Q^2<$ 6.8 GeV^2 and 1.7 $<$W$<$ 2.5 GeV. We conclude that the cross section for $\phi\pi^+\pi^-$ production is substantial.

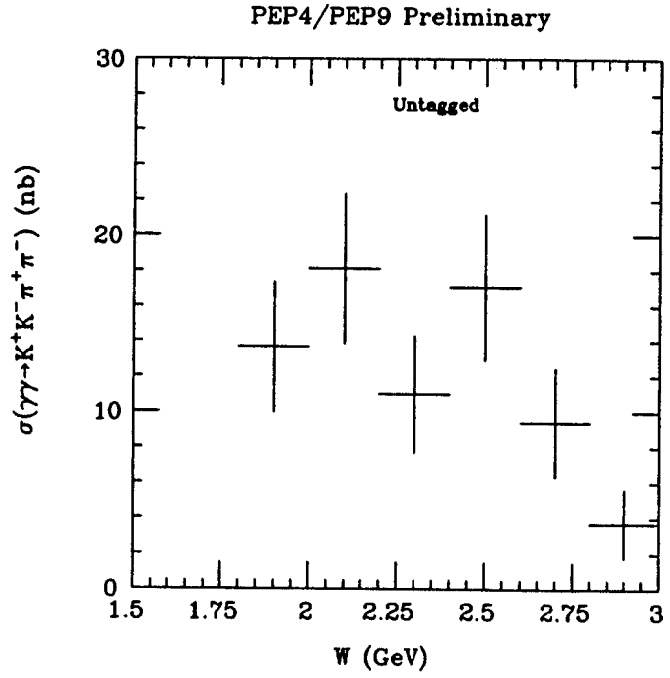

Fig.6 : Cross section calculated for $K^+K^-\pi^+\pi^-$ events. Acceptance has been determined assuming phase space production.

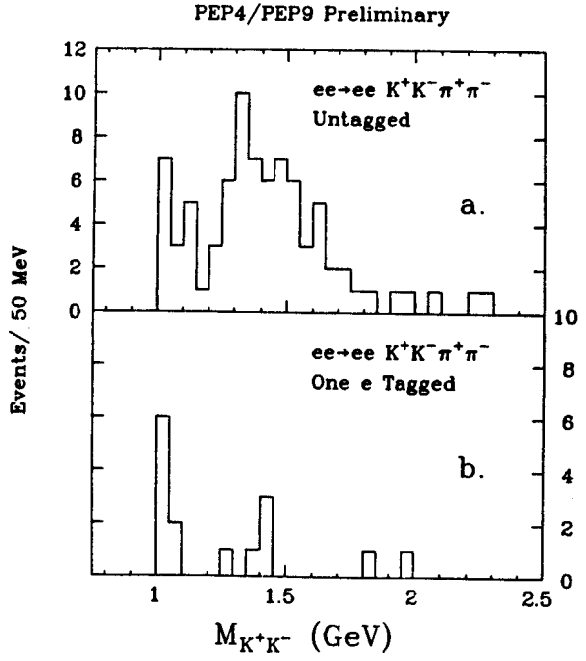

Fig.7 : The mass of K^+K^- for a. the untagged sample, and b. the tagged sample.

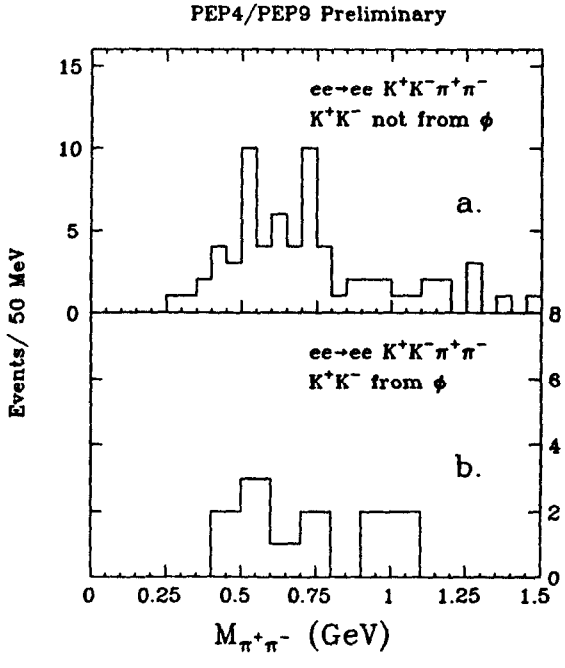

Fig.8 : a. The $\pi^+\pi^-$ masses for events without ϕs, i.e., M(K^+K^-)> 1.04 GeV. b. Events with ϕs, i.e., M(K^+K^-)< 1.04 GeV. This plot includes both tagged and untagged events.

Events containing ϕ's, i.e. those for which M(KK)< 1.04 GeV, are now removed from the $K^+K^-\pi^+\pi^-$ sample. Figure 9 a shows the scatter plot of unlike-sign Kπ combinations. Comparison with the corresponding like-sign plot indicates that no significant amount of $K^{*0}\overline{K}^{*0}$ is present. However, there is evidence for $K^{*0}K\pi$, as shown in the comparison of Figs. 9 b and c, the projections of the unlike- and like-sign Kπ combinations respectively. A clear peak at the K^{*0} mass is seen, which moreover continues to be present if events in the mass region corresponding to $K^{*0}\overline{K}^{*0}$ are removed from the plot, as seen in Fig. 9 d. Fractions of $K^{*0}\overline{K}^{*0}$, $K^{*0}K\pi$, and $K^+K^-\pi^+\pi^-$ are evaluated by comparing a correlation plot of the $K^\pm\pi^\mp$ data to plots for each of these three hypotheses generated assuming isotropic production and decay of the K^{*0}. The $K^{*0}K\pi$ fraction is 37 ± 13%. The $K^{*0}\overline{K}^{*0}$ fraction is consistent with zero; we set an upper limit of 3.4 nb (95% confidence level) for the mass region of Fig. 6. Angular distributions of the K^* in the two photon system and of the K in the K^* system show only weak anisotropies.

In conclusion, a cross section is given for $K^+K^-\pi^+\pi^-$ production. The reaction $\gamma\gamma \to \phi\rho$ is not observed, but $\gamma\gamma \to \phi\pi\pi$ is seen and a cross section is determined for tagged events. An upper limit of 3.4 nb is found for $\gamma\gamma \to K^{*0}\overline{K}^{*0}$, and the reaction $\gamma\gamma \to K^{*0}K\pi$ is observed.

IV.3 Q^2 DEPENDENCE IN $\gamma\gamma \to \pi^+\pi^-\pi^+\pi^-$.

The number of events measured in the $e^+e^- \to e^+e^-\pi^+\pi^-\pi^+\pi^-$ process can

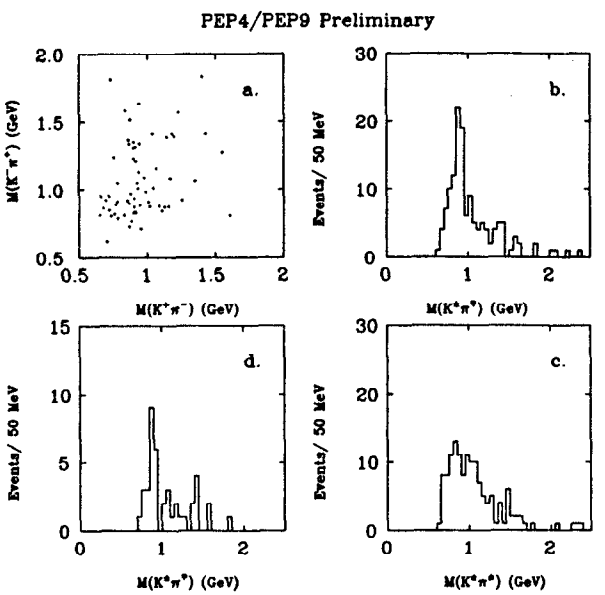

Fig.9 : a. Correlation plot of $K^+\pi^-$ versus $K^-\pi^+$ for the untagged $K^+K^-\pi^+\pi^-$ sample.
b. Projection of unlike-sign $K\pi$ combinations.
c. Projection of like-sign $K\pi$ combinations.
d. Unlike-sign combinations if the other combination has a mass greater than 1.1 GeV.

be expressed as

$$\frac{\partial^2 N}{\partial Q^2 \partial W} = L_{int}\ L_{TT}\ \sigma_{\gamma\gamma\to 4\pi}(Q^2,W)\ A(Q^2,W).$$

In this equation, L_{int} is the total integrated e^+e^- luminosity, L_{TT} is the $\gamma\gamma$ flux function and A is the product of detection and reconstruction efficiency.

A Monte Carlo integration was used to calculate A. Events were generated for the processes $\gamma\gamma \to \rho^0\rho^0$, $\rho^0\pi^+\pi^-$, 4π, with isotropic angular distributions of the ρ^0's in the $\gamma\gamma$ center of mass and the π's in the ρ^0 center of mass. Subsequently, these events were run through a detector simulation and the same off-line code that had analyzed and selected the data. The flux factor L_{TT} is calculated by numerical integration of the transverse-transverse $\gamma\gamma$ luminosity functions[5] in Q^2 and W bins. The cross section $\gamma\gamma \to \pi^+\pi^-\pi^+\pi^-$ is shown in Fig. 10 for the $Q^2 \approx 0$ data, together with data from two ranges of $Q^2 \neq 0$. The peaked structure is seen to persist for non-zero Q^2. The Q^2 dependence of $\sigma(\gamma\gamma \to \pi^+\pi^-\pi^+\pi^-)$, averaged over $1.2 < W < 2.4$ GeV is given in Fig. 11. For comparison, a simple ρ-pole form factor $1/(1+(Q^2/m_{\rho^2}))^2$, normalized to the $Q^2 = 0$ point is given. The data are seen to deviate from this behavior above $Q^2 \approx 2.0$ GeV. A contribution from the longitudinal-transverse cross section at $Q^2 > 0$ is not expected to change this curve by much. An arbitrarily normalized curve of the process $\gamma\gamma \to \mu\mu$ at W = 1.8 GeV is given also.[23] The comparison of the data with the two curves indicates a possible transition from soft to hard scattering in the $\gamma\gamma \to \pi^+\pi^-\pi^+\pi^-$process. Figures 12 a and b show the pair-mass plots for $Q^2 \approx 0$ and for a mass range W > 1.5 GeV, to be compared with Figs 12 c and d

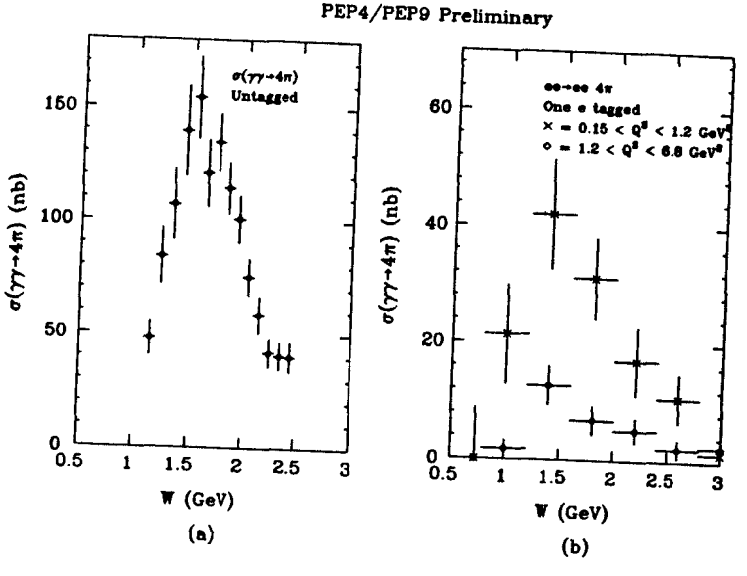

*Fig.*10 : Cross section $\sigma(\gamma\gamma \to \pi^+\pi^-\pi^+\pi^-)$ versus the mass of the $\gamma\gamma$ system.
a. $Q^2 \approx 0$.
b. $0.15 < Q^2 < 1.2$ GeV^2 and $Q^2 > 1.2$ GeV^2.

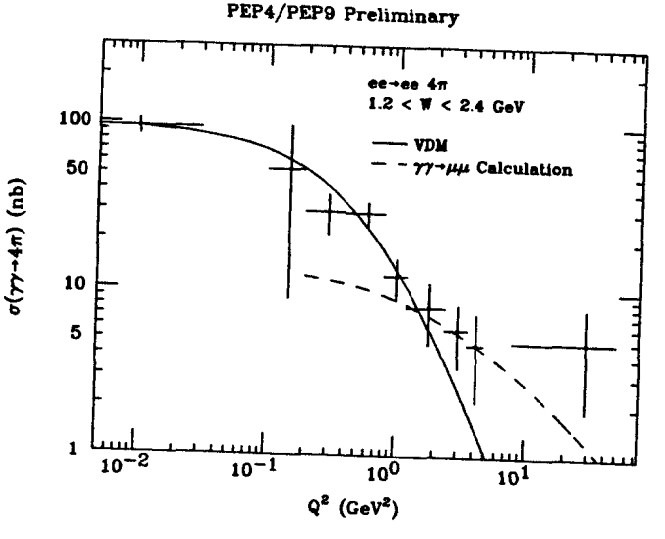

*Fig.*11 : The Q^2 dependence of the process $\gamma\gamma \to \pi^+\pi^-\pi^+\pi^-$, for $1.2 < W < 2.4$ GeV.
Solid curve: ρ-pole form factor normalized to $Q^2 = 0$.
Dashed curve: Q^2 dependence of $\gamma\gamma \to \mu\mu$, arbitrary normalization.

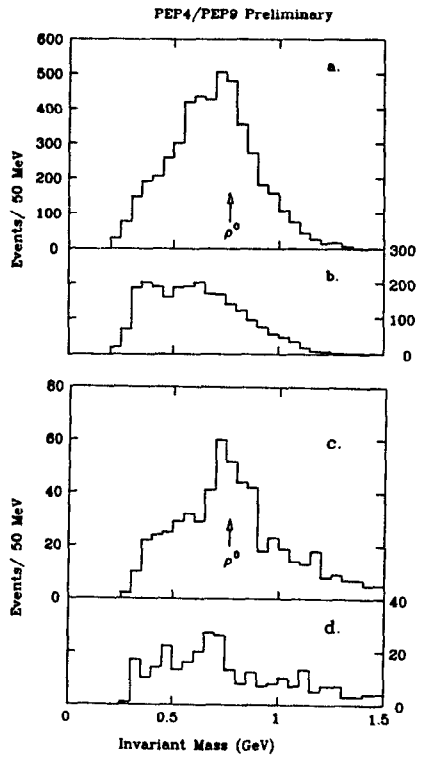

Fig.12 : a. The $\pi^+\pi^-$ mass spectrum for $Q^2 \approx 0$ and for W> 1.5 GeV.
b. The $\pi^+\pi^+$ or $\pi^-\pi^-$ mass spectrum for the same conditions.
c. The $\pi^+\pi^-$ mass spectrum for $Q^2 \neq 0$ and for W> 1.5 GeV.
d. The $\pi^+\pi^+$ or $\pi^-\pi^-$ mass spectrum for the same conditions.

for $Q^2 \neq 0$. An obvious signal at the ρ mass remains visible in the $Q^2 \neq 0$ range in the opposite charged pair combinations.

V. Summary

We reached the following conclusions:

i) The total hadronic cross section $\sigma(\gamma\gamma \rightarrow \text{hadrons})$ is approximately flat for $2 \leq W \leq 20$ GeV; photon-photon scattering thus shows the characteristics of hadron-hadron collisions in its W dependence, moreover the result is close to the factorization prediction. Its Q^2 dependence is well described by a GVD model that also describes inelastic ep scattering.

ii) In the exclusive process $\gamma\gamma \rightarrow K^+K^-\pi^+\pi^-$ we found evidence for $\phi\pi\pi$ and $K^*K\pi$ production for the first time. The $\phi\pi\pi$ cross section is larger than expected from VMD and Pomeron exchange. We found no evidence for $\phi\rho$ and $K^{*0}\overline{K}^{*0}$ production; $\rho^0\rho^0$ thus remains the only known case of vector meson pair production in $\gamma\gamma$ collisions.

iii) The Q^2 dependence of the process $\gamma\gamma \rightarrow \pi^+\pi^-\pi^+\pi^-$ in the range $0 < Q^2 < 50$ GeV^2 shows a ρ form-factor type behavior out to 2 GeV^2 and it flattens out beyond.

REFERENCES

1) *PEP-9 Two Gamma Collaboration:*
J.C. Armitage, A. Buijs, M.A. van Driel, F.C. Erné, W.G.J. Langeveld, F.L. Linde, H.P. Paar, J.C. Sens, J. Timmer, B. van Uitert, *NIKHEF, Amsterdam, the Netherlands*;
M.P. Cain, Winston Ko, R.L. Lander, D.E. Pellett, K. Maeshima, R.R. McNeil, J.R. Smith, W. Wagner, M.C.S. Williams, *University of California, Davis*;
A.M. Eisner, B.D. Magnuson, D.A. Palmer, M.K. Sullivan, *University of California Institute for Research at Particle Accelerators*;
D.L. Bintinger, G.E. Masek, K.H. Kees, E.S. Miller, J.R. Thompson, W. Vernon, J.T. White, *University of California, San Diego*;
D.O. Caldwell, U.P. Joshi, A. Lu, K.A. Schwitkis, S.J. Yellin, *University of California, Santa Barbara.*

2) *PEP-4 TPC Collaboration:*
M. Alston-Garnjost, A. Barbaro-Galtieri, A.V. Barnes, A.D. Bross, O. Chamberlain, A.R. Clark, A. Cordier, O.I. Dahl, C.T. Day, K.A. Derby, P.H. Eberhard, D.L. Fancher, B. Gabioud, J.W. Gary, N.J. Hadley, H.J. Hilke, W. Hofmann, J.E. Huth, H. Iwasaki, H.S. Kaye, R.W. Kenney, L.T. Kerth, S.C. Loken, G.R. Lynch, R.J. Madaras, R.M. Majka, P.S. Martin, J.N. Marx, W. Moses, P. Nemethy, D.R. Nygren, P.J. Oddone, M. Pripstein, P.R. Robrish, M.T. Ronan, R.R. Ross, F.R. Rouse, R.R. Sauerwein, G. Shapiro, M.D. Shapiro, M.L. Stevenson, R. van Tyen, H. Videau, E.M. Wang, W.A. Wenzel, *Lawrence Berkeley Laboratory, University of California, Berkeley*;
C.D. Buchanan, J.M. Hauptman, R.I. Koda, D.A. Park, W.E. Slater, D.H. Stork, H.K. Ticho, R.F. van Daalen Wetters, M.R. Wayne, *University of California, Los Angeles*;
W. Gorn, K.K. Kwong, J.G. Layter, C.S. Lindsey, S.O. Melnikoff, B.C. Shen, G.J. VanDalen, *University of California, Riverside*;
D.H. Badtke, J.A. Bakken, B.A. Barnett, B.J. Blumenfeld, C-Y. Chien, J. Hylen, X-Q. Lu, L. Madansky, J.A.J. Matthews, A. Pevsner, W-M. Zhang, *Johns Hopkins University, Baltimore*;
R.R. Kofler, *University of Massachusets, Amherst*;
H. Aihara, J. Chiba, H. Fujii, T. Fujii, T. Kamae, K. Maruyama, N. Toge, H. Yamamoto, M. Yamauchi, *University of Tokyo, Tokyo, Japan.*

3) H. Aihara et al. (PEP4/TPC Collaboration) *IEEE Trans. Nucl. Sci.* **30**, 63,67,76,117,153 (1983).

4) Ch. Berger et al., *Phys. Lett.* **89B**, 120(1979), **99B**, 287 (1981).

5) V.E.Balakin, V.M.Budnev, I.F.Ginzburg, *JETP Lett.* **11**, 388 (1970); G.Bonneau, M.Gourdin and F.Martin, *Nucl. Phys.* **B54**, 573 (1973); V.M.Budnev et al., *Physics Reports* **15C**, 181 (1974).

6) M.P. Cain et al., to be published in *Phys. Lett.* (1984).

7) Y.S.Tsai, **SLAC-PUB-3129.**

8) J.J.Sakurai *Phys. Rev. Lett.* **22**, 981 (1969);
J.J.Sakurai and D. Schildknecht, *Phys. Lett.* **40B**, 121 (1972).
Model II is used with:

$$f_T(q^2) = \sum_V r_V (1 - q^2/m_V^2)^{-2} + r_c(1 - q^2/1.4^2)^{-1}$$
$$f_S(q^2) = 0.25 \sum_V r_V (1 - q^2/m_V^2)^{-2}(-q^2/m_V^2)$$

$r_V = 0.65, 0.08, 0.05$ for $V = \rho, \omega, \phi$ respectively. $r_c = 0.22$. Ginzburg and Serbo, *Phys. Lett.* **109B**, 231 (1983) use this parameterization but set $\epsilon_1 = \epsilon_2 = 1$ in Eq.(2). This changes the extrapolation to $q^2 = 0$ by +5%.

9) The $f_T(q^2) = (1 - q^2/m_\rho^2)^{-2}$; $f_S(q^2) = 0.25 f_T(q^2)(-q^2/(-q^2 + m_\rho^2))$.

10) J.L.Rosner ISABELLE *Physics Prospects, BNL* rep. **17522**, 316 (1972).

11) G.Alexander, U.Maor and C.Milstene, *Phys. Letters* **131B**, 224 (1983).

12) R.Brandelik et al., *Phys. Lett.* **97B**, 448 (1980).

13) M.Althoff et al., *Z. Phys.* **C16**, (1982).

14) D.L.Burke et al., *Phys. Lett.* **100B**, 153 (1981).

15) H.J.Behrend et al., *Z. Physik* **C21**, 205 (1984).

16) H. Kolanoski, **Proceedings of the 5th International Colloquium on $\gamma\gamma$ Interactions**, Aachen, Ed. Ch. Berger, Lecture Notes in Physics, Vol. 191, Springer Verlag (1983).

17) R.L.Jaffe and K.Johnson, *Phys. Letters* **60B**, 201 (1976);
R.L.Jaffe, *Phys. Rev. D* **15**, 267 (1977).

18) B.A. Li and K.F. Liu, *Phys. Rev. D* **30**, 613 (1984), *Phys. Letters* **118B**, 435 (1982), *Phys. Rev. Letters* **51**, 1510 (1983).

19) N.N. Achasov, S.A. Devyanin, and G.N. Shestakov, *Phys. Lett.* **108B**, 134(1982).

20) C.Schmidt, private communication.

21) G.Alexander et al., *Phys. Rev. D* **26**, 1198 (1982).

22) J.E.Olsson, **Proceedings of the 5th International Colloquium on $\gamma\gamma$ Interactions**, Aachen, Ed. Ch. Berger, Lecture Notes in Physics, Vol 191, Springer Verlag (1983).
E. Hilger, **Proceedings of the 14th International Symposium on Multiparticle Dynamics**, Lake Tahoe (1983).
H. Kolanoski, Presentation at the XXII International Conference on High Energy Physics, Leipzig, July 1984.

23) V.M.Budnev et al., *Physics Reports* **C15** (1975), Appendix E.